

**$^{58}\text{Ni}$ : An Unpaired Band Crossing at New Heights of Angular Momentum for Rotating Nuclei**

D. Rudolph,<sup>1</sup> B. G. Carlsson,<sup>2</sup> I. Ragnarsson,<sup>2</sup> S. Åberg,<sup>2</sup> C. Andreoiu,<sup>1,\*</sup> M. A. Bentley,<sup>3,†</sup> M. P. Carpenter,<sup>4</sup> R. J. Charity,<sup>5</sup> R. M. Clark,<sup>6</sup> M. Cromaz,<sup>6</sup> J. Ekman,<sup>1</sup> C. Fahlander,<sup>1</sup> P. Fallon,<sup>6</sup> E. Ideguchi,<sup>5,‡</sup> A. O. Macchiavelli,<sup>6</sup> M. N. Mineva,<sup>1</sup> W. Reviol,<sup>5</sup> D. G. Sarantites,<sup>5</sup> D. Seweryniak,<sup>4</sup> and S. J. Williams<sup>3,§</sup>

<sup>1</sup>*Department of Physics, Lund University, S-22100 Lund, Sweden*

<sup>2</sup>*Department of Mathematical Physics, Lund Institute of Technology, S-22100 Lund, Sweden*

<sup>3</sup>*School of Chemistry and Physics, Keele University, Keele, Staffordshire, ST5 5BG, United Kingdom*

<sup>4</sup>*Physics Division, Argonne National Laboratory, Argonne, Illinois 60439, USA*

<sup>5</sup>*Chemistry Department, Washington University, St. Louis, Missouri 63130, USA*

<sup>6</sup>*Nuclear Science Division, Lawrence Berkeley National Laboratory, Berkeley, California 94720, USA*

(Received 15 August 2005; published 8 March 2006)

High-spin states in  $^{58}\text{Ni}$  have been investigated by means of the fusion-evaporation reaction  $^{28}\text{Si}(^{32}\text{S}, 2p)^{58}\text{Ni}$  at 130 MeV beam energy. Discrete-energy levels are observed in  $^{58}\text{Ni}$  at record-breaking 42 MeV excitation energy and angular momenta in excess of  $30\hbar$ . The states form regular rotational bands with unprecedented high rotational frequencies. A comparison with configuration dependent cranked Nilsson-Strutinsky calculations reveals an exceptional two-band crossing scenario, the interaction strength of which is strongly shape dependent.

DOI: [10.1103/PhysRevLett.96.092501](https://doi.org/10.1103/PhysRevLett.96.092501)

PACS numbers: 21.60.Cs, 23.20.En, 23.20.Lv, 27.40.+z

Rotating objects in the Universe range from galaxy clusters with about one revolution per  $10^{10}$  years to mesons with about  $10^{23}$  revolutions per second. Matter in the form of atomic nuclei approaches these most rapid rotations, and it is readily available to study the immense effects of rotation-induced forces in the quantum world. In turn, valuable clues on the effective forces acting inside the nucleus can be derived.

During the past decade, multifold high-resolution  $\gamma$ -ray spectroscopy at large  $4\pi$  germanium detector arrays yielded a plethora of new phenomena concerned with fast rotating atomic nuclei. One specific feature is that pairing between nucleons becomes less important at high angular momenta and *unpaired* band crossings may appear. While paired band crossings are generally seen at low but similar rotational frequencies in sequences of nuclei, unpaired band crossings depend on details of the nuclear spectrum at high angular momenta [1]. They can involve the exchange of one ( $1p-1h$ ) [2] or two ( $2p-2h$ ) [3,4] particles and holes. Measuring interaction strengths in  $2p-2h$  crossings provides information on forces beyond the nuclear mean field, i.e., residual interactions. These play a crucial role in the understanding of phenomena of heated rotating nuclei, such as rotational damping and the onset of chaos [5,6]. On the other hand, the  $1p-1h$  crossings are induced by Coriolis and centrifugal forces and may be described by the rotating nuclear mean field. The corresponding interaction strengths thus depend on specific features of this mean field, for example, deformation or rotational frequencies. Therefore, the observation and study of band interactions of fast rotating nuclei probe the effective nuclear theories in hitherto unknown regimes of the energy-spin plane.

In this Letter we present new results on  $^{58}\text{Ni}$  with record heights of discrete-energy  $\gamma$ -ray spectroscopy in terms of

excitation energy,  $E_x$ , angular momentum,  $I$ , and rotational frequency,  $\hbar\omega \sim E_\gamma/2$ . Previously, one high-spin rotational band in  $^{58}\text{Ni}$  was found to partially decay by discrete-energy  $\alpha$ -particle emission [7]. Preliminary analyses of data on  $^{58}\text{Ni}$  from other than the present experiments reveal an extensive level scheme of spherical and normally deformed structures [8], and indicate some ten partial particle-decaying states at the bottom of strongly deformed rotational bands [9]. Here, we shall focus on the characteristics of the highest-spin rotational bands themselves. In particular, the interaction strength between two crossing bands is found to be a prime indicator of the assigned deformation.

The present work is based on data from two almost identical experiments performed at Lawrence Berkeley National Laboratory and Argonne National Laboratory. Details can be found in Refs. [10]. In short, both experiments employed the fusion-evaporation reaction  $^{32}\text{S} + ^{28}\text{Si}$  at 130 MeV beam energy. Enriched  $0.5 \text{ mg/cm}^2$   $^{28}\text{Si}$  targets supported with either  $\sim 1 \text{ mg/cm}^2$  Ta or Au foils facing the beam were used. The  $\gamma$  rays were detected in the Gammasphere array [11], which comprised 78 Ge detectors. Heavimet collimators were removed. The  $4\pi$  CsI-array Microball [12] served the detection of light charged particles, while a Neutron Shell [13], consisting of 30 liquid-scintillator detectors, enables the detection of evaporated neutrons and thus allows the study of weak reaction channels at and beyond the  $N = Z$  line [14].

The reaction leads to  $^{58}\text{Ni}$  nuclei following the evaporation of only two protons from the compound nucleus  $^{60}\text{Zn}$ , which is formed at an excitation energy of some 64 MeV and angular momenta up to about  $38\hbar$ . At these values, most of the reaction cross section goes into three- or four-particle evaporation channels. However, if  $^{58}\text{Ni}$  is formed—this is the case for less than 1% of the re-

actions—it will be created at high excitation energies and angular momenta. The excitation scheme of  $^{58}\text{Ni}$  in Fig. 1, which is derived from the present data set, reflects this idea: It shows discrete states up to spin  $I = 32\hbar$  at record-breaking 42 MeV excitation energy. In fact, these numbers leave very little phase space for the energies of the two protons and “statistical”  $\gamma$ -ray feeding at the very top of the level scheme. Note that the system  $^{58}\text{Ni} + 2p$  lies 8.5 MeV above the ground state of  $^{60}\text{Zn}$ .

The partial level scheme in Fig. 1 was constructed using high-fold  $\gamma$ -ray events selected by two protons detected in coincidence in Microball. However, such events comprise, almost exclusively,  $\gamma$  rays from other, much stronger reaction channels with higher charged-particle multiplicity, since one or more particles may escape the detection. Therefore, it is necessary to employ the total-energy-selection method [15] to discriminate  $\gamma$  rays from  $^{58}\text{Ni}$  against the “background” of other reaction channels in the two-proton gated spectra. In short, restrictions on both the correlated charged-particle and  $\gamma$ -ray energies as well as  $\gamma$ -ray fold are imposed. To improve the  $\gamma$ -ray energy resolution an event-by-event kinematic reconstruction method was used to reduce the effect of the Doppler broadening due to the evaporated particles.

Some representative results are displayed in the  $\gamma$ -ray spectra of Fig. 2. Panel (a) shows band 1 of Fig. 1. This is the previously known rotational structure [7], which is extended by three more high-energy transitions. Besides the members of the rotational band, transitions between the low-lying near-spherical states of the  $^{58}\text{Ni}$  decay scheme are present, as well as the two weak connections to band 2

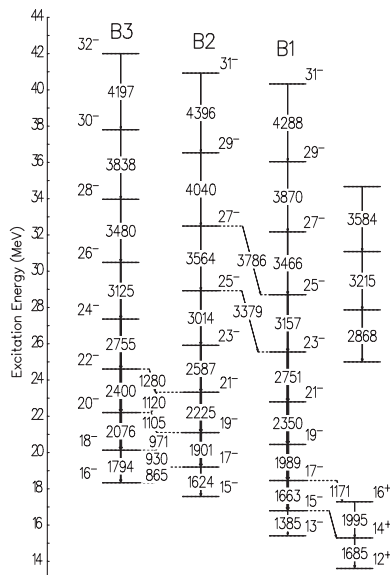


FIG. 1. Partial decay scheme of  $^{58}\text{Ni}$  from the present study. Energy labels are in keV, and the widths of the arrows correspond to the relative intensities of the  $\gamma$  rays. Note that both the energies and angular momenta of the rotational bands can be established via  $\gamma$ - and particle-linking transitions from parallel investigations on  $^{58}\text{Ni}$  [7–9].

at 3379 and 3786 keV. These are highlighted in Fig. 2(b), which otherwise illustrates the high-energy regime of band 2 by means of a sum of gates on the 4040 keV  $29^- \rightarrow 27^-$  and 4396 keV  $31^- \rightarrow 29^-$  lines in the  $^{58}\text{Ni}$ -selected  $\gamma\gamma$  correlation matrix. An indirect confirmation of the existence of the 3379 and 3786 keV lines is the presence of the 2751 and 3157 keV transitions of band 1 in Fig. 2(b). Figure 2(c) confirms the topmost transitions of band 3: It is a spectrum in coincidence with the 3838 keV  $30^- \rightarrow 28^-$  line. Note that panels (b) and (c) are restricted to high-lying entry states. Only a subset of events is used with at least 12 detected  $\gamma$  rays having released more than 19 MeV energy, while the combined energy of the two evaporated protons was less than 15 MeV. The same method was used to ensure the topmost transitions in band 1. In addition, a seemingly rotational sequence of three weak  $\gamma$  rays can be established though not connected to the rest of the level scheme in Fig. 1.

Neither particle nor  $\gamma$ -ray linking transitions [7,9] between the rotational and the near-spherical states are observed in the present data set, partly because of the strict two-proton selection method, but mainly due to the very limited overall statistics. The latter also prevents a profound analysis of average quadrupole moments of the bands based on the residual Doppler shift method [16], while angular correlations are consistent with stretched

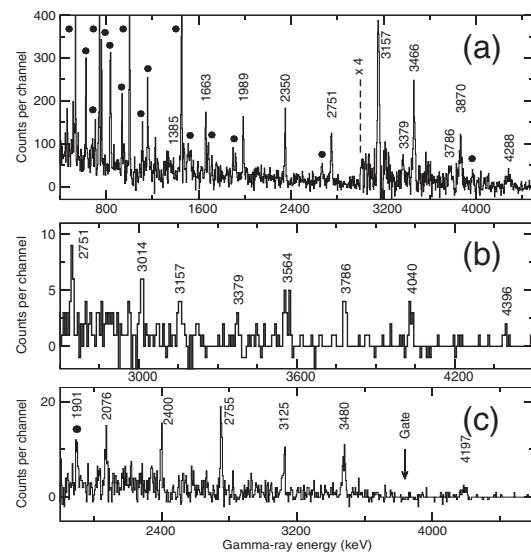


FIG. 2. Part (a) is the sum of the  $\gamma$ -ray spectra in coincidence with any combination of two different  $\gamma$  rays at 1989, 2350, 2751, 3157, 3466, or 3870 keV in band 1. Panels (b) and (c) focus on the high-energy portion of the  $\gamma$ -ray spectra in coincidence with the 4040 and 4396 keV transitions in band 2 and the 3838 keV line in band 3, respectively. All spectra are taken in coincidence with two protons detected in Microball, and summed particle and  $\gamma$ -ray energy requirements adjusted for  $^{58}\text{Ni}$  have been imposed. High-lying entry states are specifically selected for panels (b) and (c). See text for details. Energy labels are in keV and filled circles mark transitions between low-lying states in  $^{58}\text{Ni}$ .

quadrupole character. Spins, parities, and excitation energies of bands 1, 2, and 3 are well established from Refs. [7,9] and the interband transitions (cf. Fig. 1).

The observed high-spin states were analyzed using the configuration dependent cranked Nilsson-Strutinsky model (CNS) [17,18]. In this model one considers the rotation from the intrinsic frame of reference, in which the nucleons experience an additional potential caused by the Coriolis and centrifugal forces. Because of the presence of these forces the spin is forced to gradually align with the axis of rotation, which is taken to be a principal axis of the potential. The mean-field Hamiltonian

$$h^\omega = h_{\text{sp}}(\varepsilon_2, \gamma, \varepsilon_4) - \omega j_x \quad (1)$$

describes the single-particle states in the nucleus rotating with the angular velocity  $\omega$ . The first part represents the Nilsson Hamiltonian in terms of the standard quadrupole deformation parameters,  $\varepsilon_2$  and  $\gamma$ , and the hexadecapole parameter  $\varepsilon_4$ . The total energy of fixed configurations is minimized in this deformation space. At high spin, pairing is of little importance and thus neglected.

Figure 3 provides the single-particle energies in the rotating frame for a fixed deformation  $\varepsilon_2 = 0.35$  and  $\gamma = 10^\circ$  for the protons. Because of the  $N \sim Z$  nature of  $^{58}\text{Ni}$ , the neutron energies are basically identical to the proton energies. The shell gap at particle number 30 and  $\hbar\omega \approx 2.0$  MeV defines the favored neutron configuration, on which most of the observed bands are built. Indicating the dominant contributions, its configuration can be written  $\nu(f_{7/2})^{-2}(fp)^2(g_{9/2})^2$  relative to the spherical  $N = 28$  core, i.e.,  $[\nu, 22]'$  in the usual shorthand notation [18]. Figure 4 shows the observed bands together with the result of our calculation. There is only one band having one less  $g_{9/2}$  neutron. It is a strongly coupled  $\Delta I = 1$  band

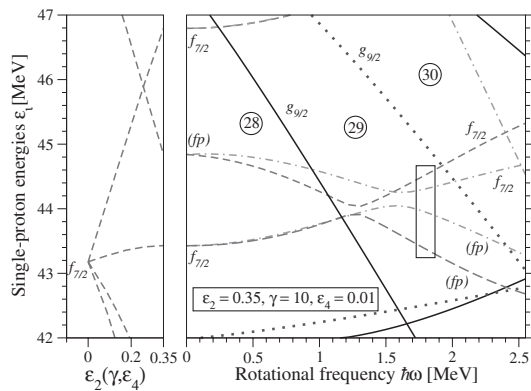


FIG. 3. Single-proton energies in the rotating frame for a prolate deformation  $\varepsilon_2 = 0.35$ ,  $\gamma = 10^\circ$ . The orbitals are labeled using the subshells with the largest amplitude in the wave function, being traced back to their spherical origin in the left panel. Lines containing dots have signature  $\alpha = -1/2$  and lines containing dashes have negative parity. The shorthand notation  $(fp)$  is used to refer to all subshells in the  $\mathcal{N} = 3$  shell except  $f_{7/2}$ .

( $[21, 11]^{0,1}$ ), the experimental counterpart of which is established as well [8].

The remaining bands differ only in their proton configurations. Those assigned to the three well-defined high-spin bands have the hole in one of the single-particle orbitals below the  $Z = 29$  gap highlighted in the box of Fig. 3. A good candidate for the fourth configuration is the unconnected band included in Fig. 1. The proton configurations can be labeled  $\pi(f_{7/2})^{-2}(fp)^1(g_{9/2})^1$  ( $[\nu 21']$ ) and  $\pi(f_{7/2})^{-3}(fp)^2(g_{9/2})^1$  ( $[\nu 31']$ ).

The two experimental high-spin bands named  $B1$  and  $B2$  approach each other around spin  $I = 25\hbar$  and then diverge again as a function of spin (see Fig. 4). Within the interaction region, the observed bands can be described as a mixture of two unperturbed bands. As these bands interact they also exchange wave functions, i.e., below  $I \approx 25\hbar$  our labeling using the occupancy of the dominating shells at high spins should be reversed.

The observed interaction involves a one-particle–one-hole excitation. Consequently, it can be described within our mean-field approach. In the calculation we have lowered the position of the proton  $f_{7/2}$  subshell by 0.4 MeV with respect to the standard CNS parameters [17] to obtain a proper splitting between the bands at  $I \sim 15\hbar$ . It is interesting to note that these bands in  $^{58}\text{Ni}$  are similar to bands previously observed in  $^{146-148}\text{Gd}$  [2,19] and  $^{140}\text{Nd}$  [20], respectively. In all cases the third ( $\Omega = 5/2$ ) orbital of an intruder high- $j$  shell interacts with the lowest orbital from the “low- $j$ ” shells. However, in the heavier nuclei, where the high- $j$  shell is  $\nu(i_{13/2})$  and  $\pi(h_{11/2})$ , respectively, only one of the two crossing bands has been observed experimentally.

The interaction strength is determined by treating the crossing as a two-level crossing. This is justified since there are no other configurations of the same signature

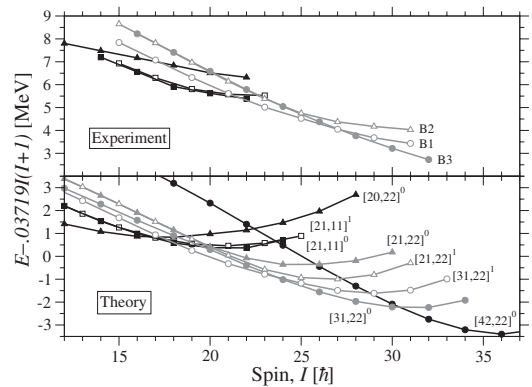


FIG. 4. Experimentally observed bands in  $^{58}\text{Ni}$  proceeding higher than spin 20 and their theoretical counterparts. Each band is given a label indicating the number of  $g_{9/2}$  particles ( $p$ ) and  $f_{7/2}$  holes ( $h$ ) along with a superscript ( $\alpha$ ) indicating the total signature of the configuration. The left side in the bracket  $[hp, hp]^\alpha$  stands for protons and the right for neutrons. As defined in the y-axis label, a reference energy of a rotating rigid body has been subtracted from the total energy.

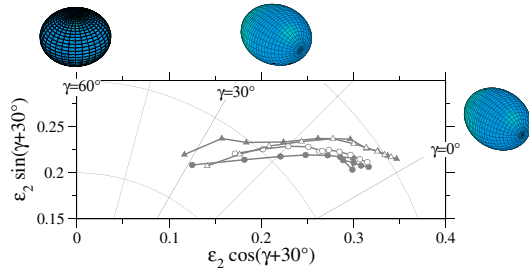


FIG. 5 (color online). Calculated deformation trajectories for the negative parity bands considered in Fig. 4. For the trajectories drawn, the deformation decreases with increasing spin. The trajectories are drawn in steps of  $\Delta I = 2\hbar$  for the spin range considered in Fig. 4.

and parity within a significant energy interval around the crossing. The two-level mixing matrix element connecting the bands  $B1$  and  $B2$  extracted from experimental energies is  $\Delta \approx 0.11$  MeV. In the calculation the interaction is somewhat weaker ( $\Delta \approx 0.10$  MeV taken from the Routhians in Fig. 3) occurring at  $I_c \sim 24\hbar$ , while it is experimentally observed at  $I_c = 25\hbar$ . The interaction strength is found to depend strongly on the  $\gamma$  deformation while the  $\varepsilon$  dependence is much weaker. Increasing and decreasing  $\gamma$  by  $\pm 10^\circ$ , the interaction strength is halved or doubled, respectively. This result is obtained when the shift of the  $f_{7/2}$  subshell is made deformation dependent such that always  $I_c \sim 24\hbar$ . Theory predicts an interaction of similar strength between the even-spin partners of the  $[31, 22]^0$  and  $[21, 22]^0$  configurations at  $I = 20\hbar$ . In the experimental data, however, there is no apparent irregularity in  $B3$ , which might indicate this interaction.

Treating  $B1$  and  $B2$  as two interacting bands connected through a matrix element of strength  $\Delta = 0.110_{-0.001}^{+0.001}$  MeV one can calculate the relative  $E2$ -transition probabilities assuming that the two bands have identical quadrupole moments and  $K$  values negligible relative to the total angular momentum. This gives predicted branching ratios,  $b$ , for intraband and interband transitions consistent with the observations: The two intense branches,  $b_{\text{th}}(B2; 27 \rightarrow B1; 25) = 0.26_{+3}^{-6}$  and  $b_{\text{th}}(B2; 25 \rightarrow B1; 23) = 0.24_{-3}^{+6}$  are seen experimentally with  $b_{\text{exp}} = 0.32(10)$  and  $b_{\text{exp}} = 0.19(4)$ , respectively. Other  $B1$ - $B2$  interband transitions cannot be firmly established, which is in line with calculated branches  $b_{\text{th}} < 0.18$ ; i.e., they fall below the observational limit (cf. Fig. 2).

Approaching the highest spins observed none of the bands terminates in an oblate aligned state at  $\gamma = 60^\circ$  [18] although  $B2$  has been observed to the maximum spin value,  $I_{\text{max}}$ , that can be built in pure configurations. Instead, the shape changes gradually from axial symmetric to triaxial shape as seen in Fig. 5 and similar to a recent high-spin study of  $^{74}\text{Kr}$  [21]. As one approaches higher spins than those observed, a configuration with one more proton in  $g_{9/2}$  is predicted to become yrast ( $[42, 22]^0$ ). This

configuration is calculated to be more deformed having  $\varepsilon_2 \approx 0.35$ – $0.45$ .

In summary, three rotational bands at exceptionally high excitation energy and angular momentum are established in  $^{58}\text{Ni}$ . They provide an outstanding example of a pure two-band unpaired crossing, since both bands are observed both above and below the crossing point. The chance for observing such phenomena is naturally greater in light nuclei where the level density is lower. Moreover, the interaction strength between the bands is found to depend significantly on the deformation parameters, and can thus be used to probe the predicted shape evolution and choice of Nilsson parameters.

Finally, we would like to thank the accelerator crews and the Gammasphere support staff at Argonne and Berkeley for their supreme efforts. The target maker, Jette Agnete Sørensen, at the Niels Bohr Institute, Copenhagen, Denmark, is also greatly acknowledged.

\*Present address: Department of Physics, University of Guelph, Guelph, Ontario, Canada N1G 2W1.

†Present address: Department of Physics, University of York, York, YO10 5DD, United Kingdom.

‡Present address: Center for Nuclear Study, University of Tokyo, Saitama 351-0198, Japan.

§Present address: School of Electronics and Physics, University of Surrey, Guildford, Surrey, GU2 7XH, United Kingdom.

- [1] G. B. Hagemann *et al.*, Nucl. Phys. A **618**, 199 (1997).
- [2] G. Hebbinghaus *et al.*, Phys. Lett. B **240**, 311 (1990).
- [3] M. A. Riley *et al.*, Phys. Rev. Lett. **60**, 553 (1988).
- [4] A. Harder *et al.*, Phys. Lett. B **374**, 277 (1996).
- [5] B. Lauritzen *et al.*, Nucl. Phys. A **457**, 61 (1986).
- [6] S. Åberg, Phys. Rev. Lett. **64**, 3119 (1990).
- [7] D. Rudolph *et al.*, Phys. Rev. Lett. **86**, 1450 (2001).
- [8] D. Rudolph *et al.*, *Proceedings of the International Symposium on Nuclear Structure Physics, Göttingen, Germany, March 2001*, edited by R. Casten *et al.* (World Scientific, Singapore, 2001), p. 161.
- [9] D. Rudolph *et al.*, Nucl. Phys. A **752**, 241c (2005).
- [10] J. Ekman *et al.*, Phys. Rev. C **70**, 014306 (2004).
- [11] I.-Y. Lee, Nucl. Phys. A **520**, 641c (1990).
- [12] D. G. Sarantites *et al.*, Nucl. Instrum. Methods Phys. Res., Sect. A **381**, 418 (1996).
- [13] D. G. Sarantites *et al.*, Nucl. Instrum. Methods Phys. Res., Sect. A **530**, 473 (2004).
- [14] J. Ekman *et al.*, Phys. Rev. C **70**, 057305 (2004).
- [15] C. E. Svensson *et al.*, Nucl. Instrum. Methods Phys. Res., Sect. A **396**, 228 (1997).
- [16] B. Cederwall *et al.*, Nucl. Instrum. Methods Phys. Res., Sect. A **354**, 591 (1995).
- [17] T. Bengtsson and I. Ragnarsson, Nucl. Phys. A **436**, 14 (1985).
- [18] A. V. Afanasjev *et al.*, Phys. Rep. **322**, 1 (1999).
- [19] I. Ragnarsson, Nucl. Phys. A **557**, 167c (1993).
- [20] A. Neusser *et al.*, Phys. Rev. C **70**, 064315 (2004).
- [21] J. J. Valiente-Dobón *et al.*, Phys. Rev. Lett. **95**, 232501 (2005).